Electronic structure and electron transport properties of Al-based $(Ni_{67}X_{33})_{1-x}Al_x$(X identical to Ti, Zr and La) amorphous alloys

1990 J. Phys.: Condens. Matter 2 541

(http://iopscience.iop.org/0953-8984/2/3/004)

J. Phys.: Condens. Matter **2** (1990) 541–557. Printed in the UK

Electronic structure and electron transport properties of Al-based $(Ni_{67}X_{33})_{1-x}Al_x$ (X ≡ Ti, Zr and La) amorphous alloys

U Mizutani†, S Ohashi†‡, T Matsuda§, K Fukamichi‖ and K Tanaka¶

† Department of Crystalline Materials Science, Nagoya University, Furo-cho, Chikusa-ku, Nagoya 464-01, Japan

§ Department of Physics, Aichi University of Education, Kariya-shi, Aichi-ken 448, Japan

‖ Department of Materials Science, Tohoku University, Sendai 980, Japan

¶ Department of Materials Science and Engineering, Nagoya Institute of Technology, Showa-ku, Nagoya 466, Japan

Received 16 June 1989, in final form July 25 1989

Abstract. A large number of $(Ni_{67}X_{33})_{1-x}Al_x$ (X ≡ Ti, Zr and La; $0 \leqslant x \leqslant 0.85$) ternary amorphous alloys have been synthesised by the melt-spinning technique in combination with the sputtering method as a supplementary tool. The electronic structure was studied through measurements of the low-temperature specific heats and the x-ray photoemission spectroscopy (XPS) spectra. For comparison, the amorphous $Al_{100-x-y}Si_xNi_y$ ($10 \leqslant x \leqslant 35$, $10 \leqslant y \leqslant 20$) alloys were also prepared and their valence band structure was studied by XPS and soft-x-ray spectroscopy. As electron transport properties, we measured the electrical resistivity, the Hall coefficient and the thermoelectric power over a wide temperature range below 300 K. We revealed that the electronic structure at the Fermi level changes from the d- to sp-electron-dominant states, as the Al content increases across $x = 0.6$. This drastic change in the electronic structure is found to be reflected in various electron transport properties and the crystallisation temperature. A reversal in the sign of the Hall coefficient and the change in the characteristic feature of the temperature dependence of the electrical resistivity have been discussed in relation to the electronic structure involved.

1. Introduction

Inoue *et al* (1987) succeeded for the first time in preparing stable Al-rich amorphous alloys in the Al–Si–X and Al–Ge–X (X ≡ Cr, Mn, Fe, Co and Ni) ternary systems by the melt-spinning method and found that some of these systems in a limited composition range possess a high ductility. Following this discovery, their group further reported a number of data concerning the vitrification of Al-rich ternary alloys, which include Al–late transition metal (TL)–early transition metal (TE) (Tsai *et al* 1988), Al–Y–TL and Al–La–TL (Inoue *et al* 1988a). They have claimed that the newly discovered ductile Al-rich amorphous alloys are potentially of practical use as a new high-strength low-density material (Inoue *et al* 1988b).

‡ Present address: Toshiba Corporation, Semiconductor Division, 1-1 Shibaura 1-chome, Minato-ku, Tokyo 105, Japan.

0953-8984/90/030541 + 17 $03.50

The Al-rich amorphous alloys are also of great interest from the point of view of the electron transport properties. Inoue *et al* (1987), for example, noted that the resistivity of the amorphous $Al_{60}Ge_{30}Ni_{10}$ alloy exceeds 1000 $\mu\Omega$ cm. This is extremely high in view of the ordinary transport theory, which tells us that the resistivity of alloys consisting of two polyvalent metals such as Al and Ge in the liquid state is approximately given by a weighted mean of those of pure constituent metals ($\rho = 24$ $\mu\Omega$ cm and 68 $\mu\Omega$ cm for liquid Al and Ge, respectively) (Faber and Ziman 1965). The electrical resistivity measurements for the liquid Al–Ge binary alloys have most recently been reported and indeed confirmed the above mentioned general feature (Gasser *et al* 1989). Being stimulated by the work of Inoue *et al*, Yamanaka *et al* (1988) studied the electronic properties of $Al_{100-x-y}Si_xNi_y$ and $Al_{90-x}Ge_xNi_{10}$ ($10 \leqslant x \leqslant 35$, $10 \leqslant y \leqslant 20$) amorphous alloys through the measurements of the low-temperature specific heat, the Hall coefficient and the electrical resistivity. It turned out that the sp electrons dominate at the Fermi level E_F, in spite of the presence of Ni, and that the electron transport properties can be consistently described in a unified picture proposed for the non-magnetic amorphous alloys (Mizutani 1988a).

In the case of Al–TL–TE ternaries, Yamada *et al* (1987b) have reported that the glass-forming range extends up to 30 at.% Al when Al is added to $Ni_{33}Zr_{67}$. Hence, we expect that a wide glass-forming range would be obtained along the line connecting the two glass-forming ranges: one at the Ni–Zr end and the other at the Al-rich end developed by Inoue and his group. The fabrication of amorphous alloys over as wide a composition range as possible is particularly needed for systematic studies of electron transport phenomena. In the present work, we prepared a large number of amorphous $(Ni_{67}Zr_{33})_{1-x}Al_x$ $(0 \leqslant x \leqslant 0.85)$, $(Ni_{67}Ti_{33})_{1-x}Al_x$ $(0.3 \leqslant x \leqslant 0.85)$ and $(Ni_{67}La_{33})_{1-x}Al_x$ $(0.7 \leqslant x \leqslant 0.85)$ ternary alloys and studied the electronic structure and the electron transport properties by measuring the low-temperature specific heat, the x-ray photoemission spectroscopy (XPS) spectrum, the electrical resistivity, the Hall coefficient and the thermoelectric power. The soft-x-ray emission as well as the XPS spectra are also measured for the $Al_{100-x-y}Si_xNi_y$ ternary amorphous alloys.

2. Experimental procedure

Alloy ingots $(Ni_{67}X_{33})_{1-x}Al_x$ (X ≡ Ti, Zr and La; $0 \leqslant x \leqslant 0.85$) and $Al_{100-x-y}Si_xNi_y$ ($10 \leqslant x \leqslant 35$, $10 \leqslant y \leqslant 20$) were prepared by arc melting of the appropriate amounts of the constituent elements Al (purity, 99.99%), Ni (purity, 99.97%), Ti (purity, 99.97%), Zr (purity, 99.97%), La (purity, 99.9%) and Si (purity, 99.999%). The amorphous alloy ribbons were fabricated by an ordinary single-roll spinning wheel apparatus operated in a reduced Ar gas atmosphere. The formation of an amorphous single phase was confirmed by x-ray diffraction with Cu Kα radiation. The $(Ni_{33}Ti_{67})_{0.7}Al_{0.3}$, $(Ni_{33}Ti_{67})_{0.5}Al_{0.5}$ and $(Ni_{67}Zr_{33})_{0.5}Al_{0.5}$ alloys were vitrified by the high-rate DC sputtering technique because of their poor glass-forming ability when subjected to the melt-spinning method. The composition was checked by electron probe microanalysis and turned out to be in good agreement with the nominal composition to within ±1%.

The low-temperature specific heat, the electrical resistivity and the Hall coefficient were measured in the temperature ranges 1.5–6 K, 2–300 K and 77–300 K, respectively. X-ray photoemission valence band spectra were obtained, using monochromated x-rays of the Al Kα line (Surface Science Instrument SSX-100). Soft-x-ray emission spectra were measured, using a bent-crystal x-ray micro-analyser (XMA) at an accelerating

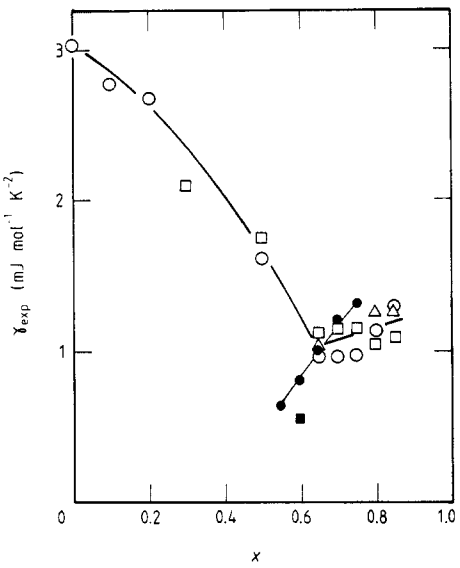

Figure 1. The electronic specific heat coefficient γ_{exp} as a function of Al content for $(Ni_{67}X_{33})_{1-x}Al_x$ ($X \equiv$ Ti (□), Zr (○) and La (△)) and $Al_{90-x}Si_xNi_{10}$ (●) and $Al_{60}Ge_{30}Ni_{10}$ (■) amorphous alloys.

voltage of 10 kV (Yamada *et al* 1987b). The crystallisation temperature T_x was determined from the temperature dependence of the resistivity at a heating rate of 10 K min^{-1}. The density was measured with the Archimedes method, using xylene as the working fluid. The thermoelectric power was measured at a heating rate of approximately 2.5 K min^{-1} in the temperature range 77–570 K, using the integration method with liquid nitrogen as a cold reservoir.

3. Results

3.1. Low-temperature specific heat

The low-temperature specific heat data in the range 1.5–6 K can be well fitted to the ordinary equation $C = \gamma T + \alpha T^3 + \delta T^5$ for all alloys studied in the present experiment. The specific heat coefficients are determined by the least-squares fitting to the above equation. The Debye temperature Θ_D is derived from α through $\Theta_D = (12\pi R/5\alpha)^{1/3}$, where R is the gas constant. The superconductivity is manifested as a jump in the specific heat only for the three alloys $(Ni_{67}Zr_{33})_{0.15}Al_{0.85}$, $(Ni_{67}La_{33})_{0.20}Al_{0.80}$ and $(Ni_{67}La_{33})_{0.15}Al_{0.85}$.

The measured electronic specific heat coefficient γ_{exp} is known to be enhanced beyond the band-structure contribution γ_{band} owing to the electron–phonon interaction. The enhancement factor λ can be estimated by inserting the measured Debye temperature Θ_D and the superconducting transition temperature T_c into the McMillan (1968) formula. The resulting value of λ turned out to be around 0.4. This cannot be corrected unless superconductivity is observed. Realising the fact that its magnitude is rather small and its composition dependence is weak, we may reasonably assume the value of γ_{exp} to be a measure of the density of states at the Fermi level.

Figure 1 shows the Al concentration dependence of γ_{exp} for the three $(Ni_{67}X_{33})_{1-x}Al_x$ ($X \equiv$ Ti, Zr and La) alloy systems together with the previously reported data for Al–Si–Ni and Al–Ge–Ni (Yamanaka *et al* 1988). A sharp contrast exists between two series of data; the value of γ_{exp} in metal–metal systems is essentially independent of the solute

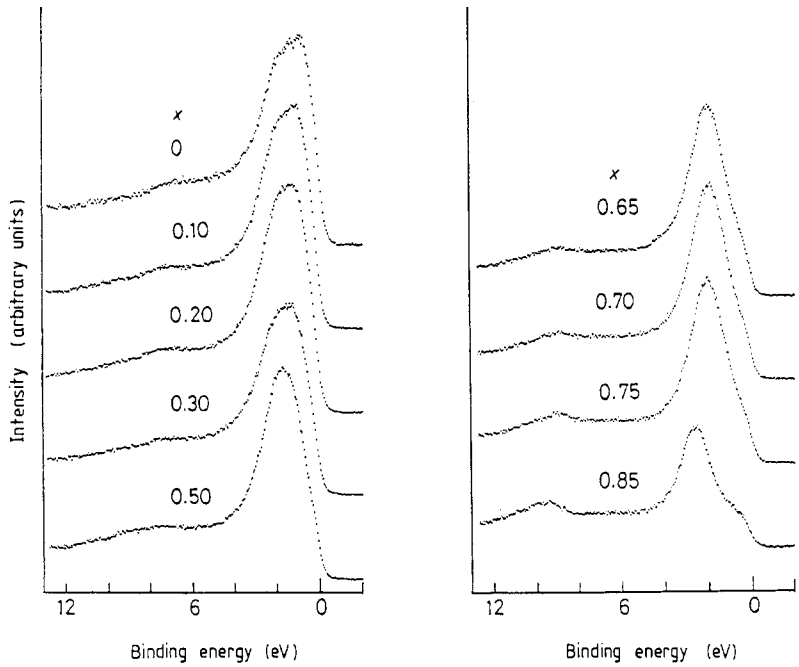

Figure 2. XPS spectra for a series of $(Ni_{67}Zr_{33})_{1-x}Al_x$ amorphous alloys over the range $0 \leqslant x \leqslant 0.85$. The Fermi level is taken as the origin of the energy axis. The Al Kα (1486 eV) line was used as an incident beam.

species Ti, Zr and La and exhibits a drastic decrease with increasing Al content up to 60 at.% with a subsequent gradual increase, whereas that in the metal–metalloid systems sharply decreases with decreasing Al content below 70 at.%.

3.2. *XPS and soft-x-ray valence band spectra*

The XPS valence band spectra for a series of $(Ni_{67}Zr_{33})_{1-x}Al_x$ and $Al_{100-x-y}Si_xNi_y$ amorphous alloys are shown in figures 2 and 3 respectively. All spectra consist of a large peak centred around 2–3 eV below the Fermi level E_F. As is clearly seen from figure 2, the peak reduces its intensity and also width with increasing Al content. Furthermore, the peak position is seen to be displaced slightly towards a higher binding energy. A small hump observed at about 9 eV is due to the O 2p and Ar 3p states, the latter of which is introduced during Ar sputtering on the surface of a specimen.

The Al Kβ and Si Kβ emission spectra for the $Al_{90-x}Si_xNi_{10}$ amorphous alloys are shown in figures 4 and 5, respectively. These spectra are known to reflect the Al 3p and Si 3p partial densities of states. The most prominent feature is that the Si Kβ spectrum gradually changes its appearance and approaches that of pure Si, when the Si content is increased to 35 at.%. In contrast, the Al Kβ spectrum in the ternary alloys maintains features characteristic of pure Al. Figure 6 shows the Ni Lα spectra for the $Al_{80-x}Si_{20}Ni_x$ amorphous alloys, together with that of pure Ni. From the spectra, we learn that the Ni 3d band in the ternary alloys is shifted to a higher binding energy, compared with that of pure Ni, which is consistent with the XPS spectra mentioned above.

3.3. *Electron transport properties*

The electrical resistivity at 300 K is shown in figure 7 as a function of Al content for all Al-based amorphous alloy systems. The value of ρ_{300K} for the three $(Ni_{67}X_{33})_{1-x}Al_x$

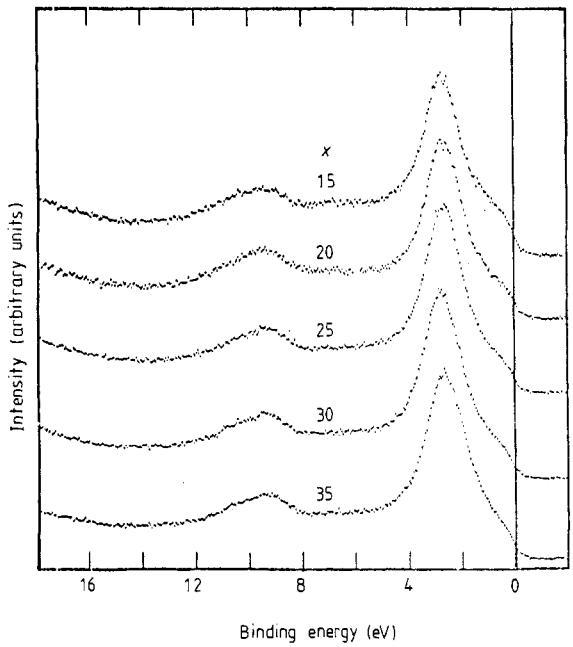

Figure 3. XPS spectra for a series of $Al_{90-x}Si_xNi_{10}$ amorphous alloys. The Fermi level is taken as the origin of the energy axis. The Al Kα (1486 eV) line was used as an incident beam.

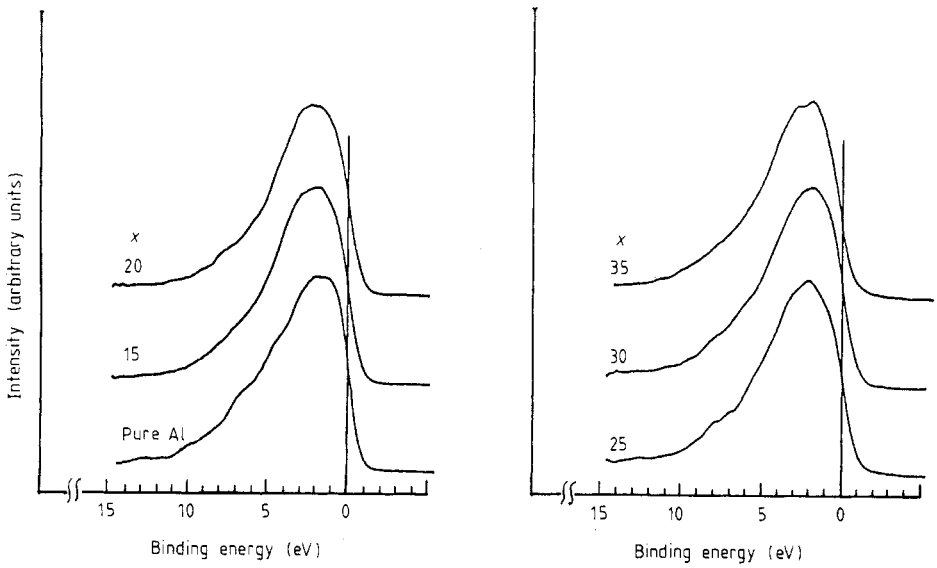

Figure 4. The soft-x-ray Al Kβ emission spectra for $Al_{90-x}Si_xNi_{10}$ amorphous alloys. The Fermi level is taken as the origin of the energy axis.

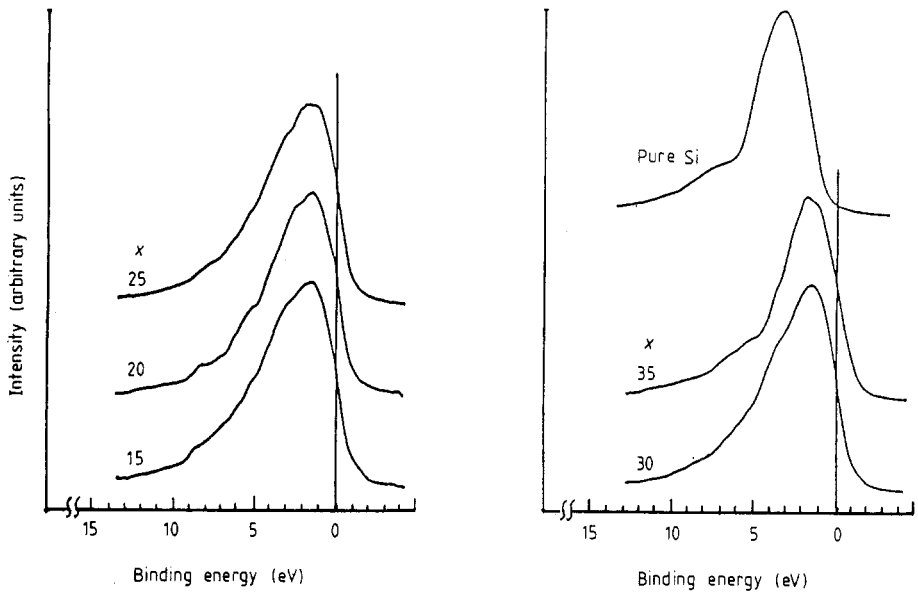

Figure 5. The soft-x-ray Si Kβ emission spectra for $Al_{90-x}Si_xNi_{10}$ amorphous alloys. The Fermi level is taken as the origin of the energy axis.

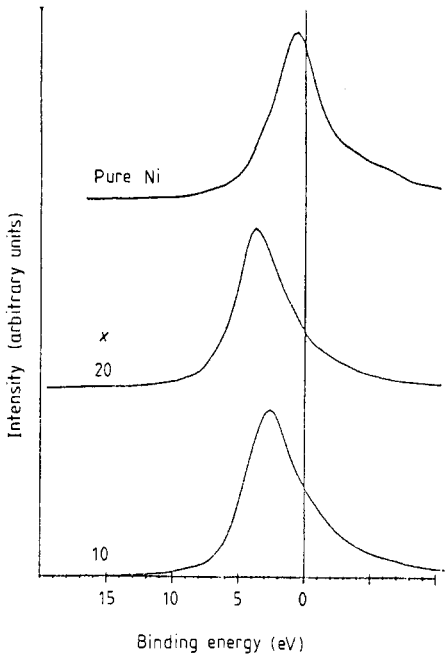

Figure 6. The soft-x-ray Ni Lα emission spectra for $Al_{80-x}Si_{20}Ni_x$ amorphous alloys. The Fermi level is taken as the origin of the energy axis.

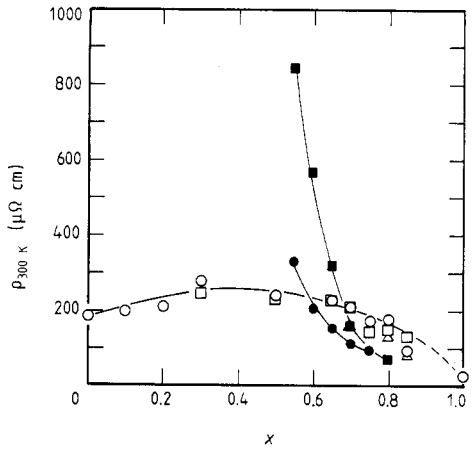

Figure 7. The electrical resistivity at 300 K as a function of Al content for $(Ni_{67}X_{33})_{1-x}Al_x$ (X ≡ Ti (□), Zr (○) and La (△)) and $Al_{90-x}Si_xNi_{10}$ (●) and $Al_{90-x}Ge_xNi_{10}$ (■) amorphous alloys. The value for Al refers to the liquid state.

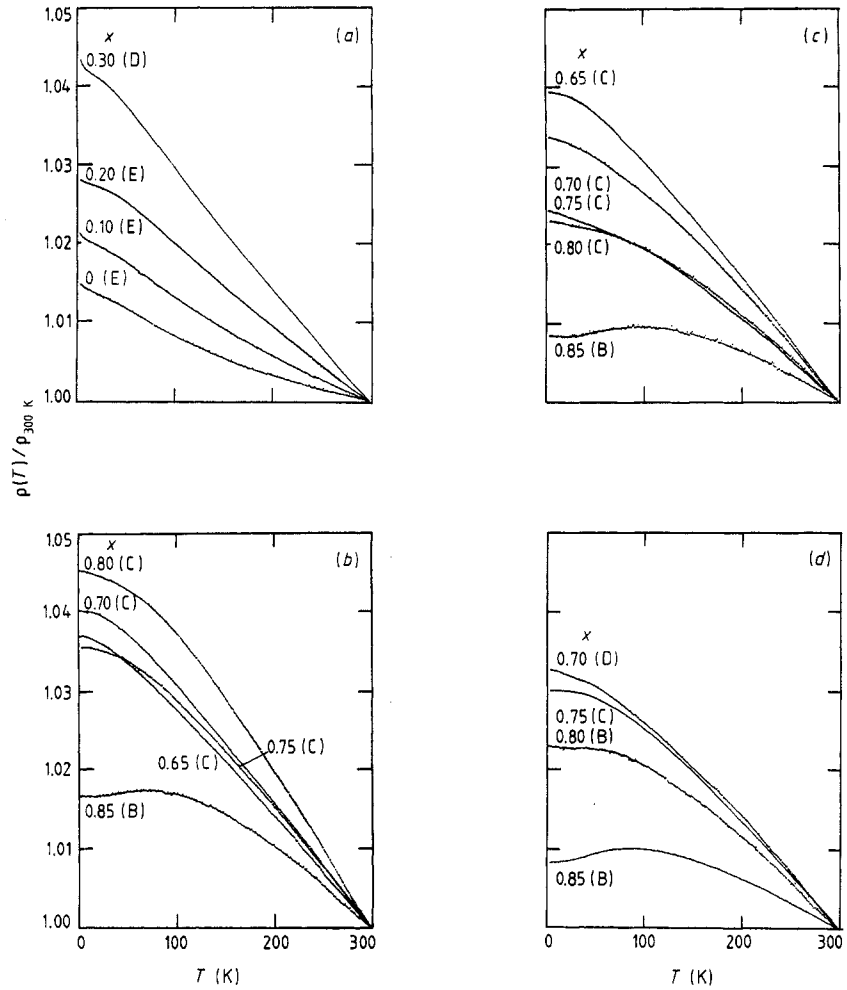

Figure 8. Temperature dependences of the electrical resistivity of (*a*) Al-poor $(Ni_{67}Zr_{33})_{1-x}Al_x$ ($0 \leq x \leq 0.30$), (*b*) Al-rich $(Ni_{67}Zr_{33})_{1-x}Al_x$ ($0.65 \leq x \leq 0.85$), (*c*) $(Ni_{67}Ti_{33})_{1-x}Al_x$ ($0.65 \leq x \leq 0.85$) and (*d*) $(Ni_{67}La_{33})_{1-x}Al_x$ ($0.7 \leq x \leq 0.85$) amorphous alloys. The resistivity is normalised with respect to that at 300 K. The letters in parentheses refer to the ρ–T curves illustrated in figure 12.

($X \equiv$ Ti, Zr and La) alloy systems is again almost independent of the atomic species X. It increases gradually on adding Al to $Ni_{67}Zr_{33}$, reaches a broad maximum at about $x = 0.3$ and subsequently decreases with further increase in Al content. On the other hand, the value of ρ in Al–Si–Ni and, particularly, in Al–Ge–Ni sharply increases with decreasing Al content below 70 at.%.

The temperature dependence of the electrical resistivity is plotted in figures 8(*a*), 8(*b*), 8(*c*) and 8(*d*) for Al-poor $(Ni_{67}Zr_{33})_{1-x}Al_x$, Al-rich $(Ni_{67}Zr_{33})_{1-x}Al_x$, $(Ni_{67}Ti_{33})_{1-x}Al_x$ and $(Ni_{67}La_{33})_{1-x}Al_x$ amorphous alloys, respectively. The ρ–T curve is concave for Al-poor alloys, whereas it is convex for Al-rich alloys. The data for Al–Si–Ni and Al–Ge–Ni have already been given in the literature (Yamanaka *et al* 1988).

The Hall coefficient R_H at 300 K is plotted in figure 9 as a function of Al content for the relevant alloy systems. The value of R_H for the metal–metal systems takes a positive

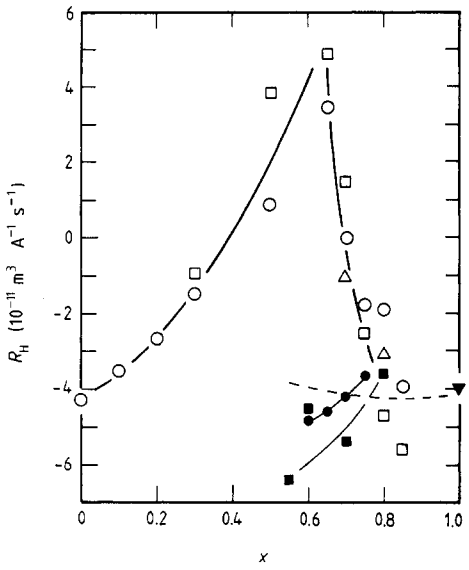

Figure 9. The Hall coefficient at 300 K as a function of Al content for $(Ni_{67}X_{33})_{1-x}Al_x$ (X ≡ Ti (□), Zr (○) and La (△)), $Al_{90-x}Si_xNi_{10}$ (●) and $Al_{90-x}Ge_xNi_{10}$ (■) amorphous alloys: ▼, data for liquid Al; – – –, curve drawn assuming the free-electron model.

sign in the region $0.4 \leqslant x \leqslant 0.7$. On the other hand, R_H for the metal–metalloid systems Al–Si–Ni and Al–Ge–Ni deviates in an opposite direction and takes more negative values with decreasing Al content below 70 at.%.

The thermoelectric power is plotted in figure 10 as a function of temperature for a series of $(Ni_{67}Zr_{33})_{1-x}Al_x$ alloys. Both its absolute value and the slope are positive in Al-poor alloys, but negative in Al-rich alloys. The value of the slope S/T determined in the vicinity of 300 K is plotted in figure 11 for the three alloy systems $(Ni_{67}X_{33})_{1-x}Al_x$ (X ≡ Ti, Zr and La) as a function of Al content x.

All relevant numerical data described in § 3 are summarised in table 1.

4. Discussion

4.1. Electronic structure

The valence band structure of the $Ni_{1-x}Zr_x$ amorphous alloys has already been well established experimentally and theoretically and is described by the two separate peaks associated with the Ni 3d band at the binding energy of about 2 eV and the Zr 4d band lying across the Fermi level (Oelhafen *et al* 1980, Nguyen Manh *et al* 1987a, b). However, as is seen from figure 2, the XPS valence band spectrum for $Ni_{67}Zr_{33}$ consists of only a single peak, which reflects mainly the Ni 3d states. In other words, the Zr 4d states are barely visible in the XPS spectrum, because the cross section for the minority element Zr is much smaller than that for the major element Ni. We believe that the density of states at E_F in $Ni_{67}Zr_{33}$ is still dominated by the Zr 4d states and that the addition of Al reduces both Zr and Ni concentrations, resulting in a reduction in the respective peak heights. This naturally explains the observed rapid decrease in γ_{exp} in figure 1 on adding Al to $Ni_{67}Zr_{33}$.

A shoulder appears in the XPS spectra at the binding energy of about 1 eV, when the Al content exceeds 0.6, and its structure becomes more evident with further increase in Al content. A similar shoulder is also visible in all Al–Si–Ni alloys. Hence, we consider

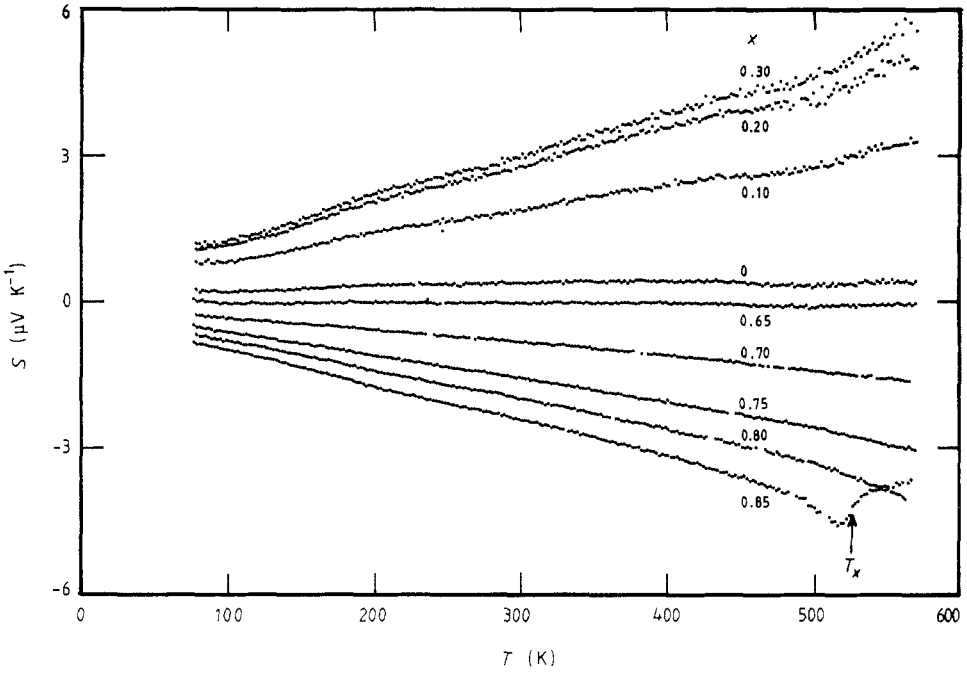

Figure 10. Temperature dependence of the thermoelectric power for a series of $(Ni_{67}Zr_{33})_{1-x}Al_x$ amorphous alloys. An arrow for the alloy with $x = 0.85$ indicates the crystallisation temperature T_x deduced from the electrical resistivity measurements (see table 1). Note the difference in the heating rate between the thermoelectric power and the resistivity measurements.

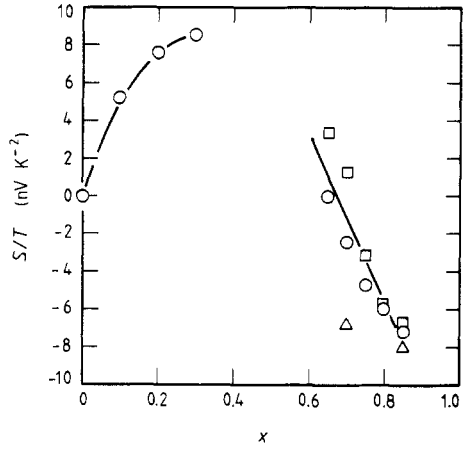

Figure 11. The value of S/T near 300 K as a function of Al content for $(Ni_{67}X_{33})_{1-x}Al_x$ ($X \equiv$ Ti (□), Zr (○) and La (△)).

that the shoulder is a characteristic feature observed in common with the Al-rich alloys. Here it should be recalled that the termination of the drastic decrease in the γ_{exp}-value shown in figure 1 also occurs at an Al concentration x of 0.6. From both XPS and specific heat data, therefore, we conclude that the Fermi level sits in the Zr 4d states up to $x = 0.6$ and that it moves into the sp band above this critical concentration. For convenience in the discussion on the electron transport, we refer to $(Ni_{67}X_{33})_{1-x}Al_x$ with $x < 0.6$ as the d-electron system and that with $x > 0.6$ and all Al–Si (or Ge)–Ni as the sp–electron system.

Table 1. Electronic properties of $(Ni_{67}X_{33})_{1-x}Al_x$ (X ≡ Ti, Zr and La) amorphous alloys. The ρ–T curve types refer to figure 12. The alloys with asterisks were prepared by sputtering; the other alloys were prepared by liquid quenching.

x	γ (mJ mol^{-1} K^{-2})	α (μJ mol^{-1} K^{-4})	δ (μJ mol^{-1} K^{-6})	Θ_D (K)	T_c (K)	ρ_{300K} ($\mu\Omega$ cm)	TCR (10^{-4} K^{-1})	ρ–T curve type	R_H (10^{-11} m^3 A^{-1} s^{-1})	S/T (nV K^{-2})	T_x (K)	d (g cm^{-3})
						X ≡ Ti						
0.30*	2.09 ± 0.02	24.3 ± 0.1	0.28 ± 0.02	431 ± 6	—	248	−1.28	E	−0.95	—	—	—
0.50*	1.74 ± 0.02	40.2 ± 0.1	−0.28 ± 0.03	364 ± 3	—	230	−1.89	D	3.85	—	761	—
0.65	1.11 ± 0.02	24.0 ± 0.1	−0.33 ± 0.03	432 ± 7	—	225	−1.85	D	4.85	3.3	678	4.13
0.70	1.14 ± 0.02	22.2 ± 0.7	−0.14 ± 0.02	444 ± 5	—	213	−1.95	D	1.50	1.3	672	3.51
0.75	1.14 ± 0.01	22.0 ± 0.7	−0.04 ± 0.16	445 ± 6	—	145	−2.16	C	−2.56	−3.2	664	3.65
0.80	1.04 ± 0.01	40.0 ± 0.1	−0.22 ± 0.03	365 ± 3	—	149	−3.56	C	−4.76	−5.8	648	2.88
0.85	1.17 ± 0.01	33.2 ± 0.7	−0.14 ± 0.02	388 ± 3	—	130	−0.91	B	−5.61	−6.6	562	3.16
						X ≡ Zr						
0	3.02 ± 0.02	62.8 ± 1.3	0.33 ± 0.03	314 ± 2	—	189	−0.22	E	−4.29	0	826	7.48
0.10	2.77 ± 0.02	63.5 ± 1.2	0.26 ± 0.03	313 ± 2	—	198	−0.62	E	−3.55	5.2	830	7.43
0.20	2.67 ± 0.03	46.9 ± 1.1	0.33 ± 0.03	346 ± 3	—	210	−1.04	E	−2.65	7.6	779	—
0.30	—	—	—	—	—	280	−1.56	E	−1.44	8.6	791	—
0.50*	1.60 ± 0.01	19.0 ± 0.7	0.37 ± 0.02	468 ± 7	—	239	−3.33	E	0.86	—	715	—
0.65	0.96 ± 0.02	19.6 ± 0.5	−0.09 ± 0.02	463 ± 4	—	227	−1.85	D	3.44	0	784	—
0.70	0.95 ± 0.02	20.8 ± 0.8	−0.05 ± 0.02	454 ± 6	—	209	−2.07	C	0.01	−2.4	744	3.74
0.75	0.97 ± 0.01	24.0 ± 0.7	−0.18 ± 0.02	433 ± 4	—	172	−1.29	C	−1.76	−4.7	690	3.06
0.80	1.13 ± 0.01	43.8 ± 1.0	−0.12 ± 0.03	354 ± 3	—	177	−2.11	C	−1.87	−6.0	640	3.33
0.85	1.30 ± 0.01	45.8 ± 1.1	0.08 ± 0.03	349 ± 3	2.12	95	−1.91	B	−3.94	−7.1	528	2.99
						X ≡ La						
0.70	1.04 ± 0.02	40.0 ± 1.0	−0.07 ± 0.03	365 ± 3	—	159	−1.93	C	−1.08	−6.7	670	—
0.75	—	—	—	—	—	150	−1.76	C	—	−9.5	665	—
0.80	1.26 ± 0.01	55.9 ± 1.2	−0.04 ± 0.03	326 ± 3	1.73	124	−1.39	B	−3.09	−9.5	603	—
0.85	1.28 ± 0.01	65.3 ± 1.2	−0.11 ± 0.03	310 ± 2	2.45	80	−0.15	B	—	−8.0	518	—

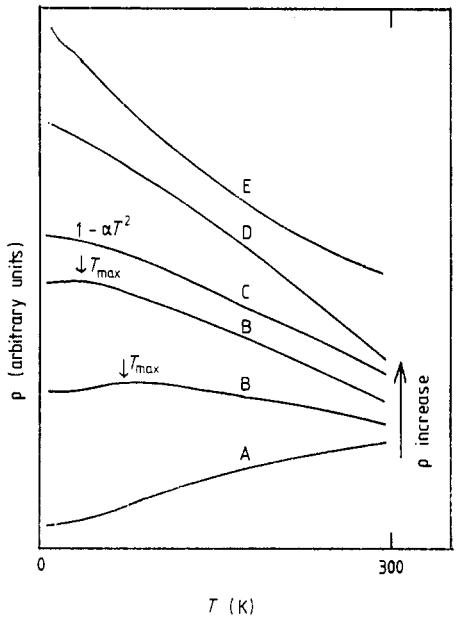

Figure 12. Schematic illustration of the ρ–T characteristics observed in general in non-magnetic amorphous alloys.

All soft-x-ray emission spectra, including both the Al Kβ and the Si Kβ spectra in figures 4 and 5, resemble that of pure Al, except for the Si Kβ spectra for the 35 at.% Si alloy. This indicates that the Al and Si 3p electrons form a free-electron-like common band, as long as the Si content is below about 30 at.%. In contrast, the Si Kβ spectrum for the 35 at.% Si alloy is much thinner and resembles more that of pure Si, providing good evidence for the development of appreciable covalent bonding with increasing Si content.

4.2. Electron transport mechanism

Mizutani (1988a) presented a unified picture for the electron transport mechanism in non-magnetic amorphous alloys. Any ρ–T dependence below 300 K in non-magnetic amorphous alloys can be described by one of the five representative forms, which are reproduced in figure 12. A positive TCR occurs over a whole temperature range, as long as the resistivity is low. This is shown as curve A in figure 12. When the resistivity is increased, a negative TCR appears in a high-temperature range and progressively extends its region towards low temperatures with further increase in resistivity. This naturally results in a resistivity maximum in the intermediate-temperature range, as denoted by curve B. Eventually, a negative TCR dominates over the whole temperature range, the ρ–T curve being well fitted to a T^2-dependence at low temperatures and a T-dependence at high temperatures. Curve C is a limiting form predicted from the generalised Faber–Ziman theory, which is constructed on the basis of the Boltzmann transport equation. The electron mean free path in alloys, whose ρ–T is characterised by either curve D or curve E, is found to be almost equal to the average atomic distance. Curves D and E cannot be explained within the framework of the Boltzmann transport equation. Indeed, weak localisation coupled with the enhanced electron–electron interaction is suggested (Mizutani *et al* 1988, Sakamoto *et al* 1988).

The conductivity σ is generally expressed in the form

$$\sigma = \rho^{-1} = e^2 v_F \Lambda_F N(E_F)/3 \tag{1}$$

where v_F is the average Fermi velocity of the conduction electrons, Λ_F is the mean free

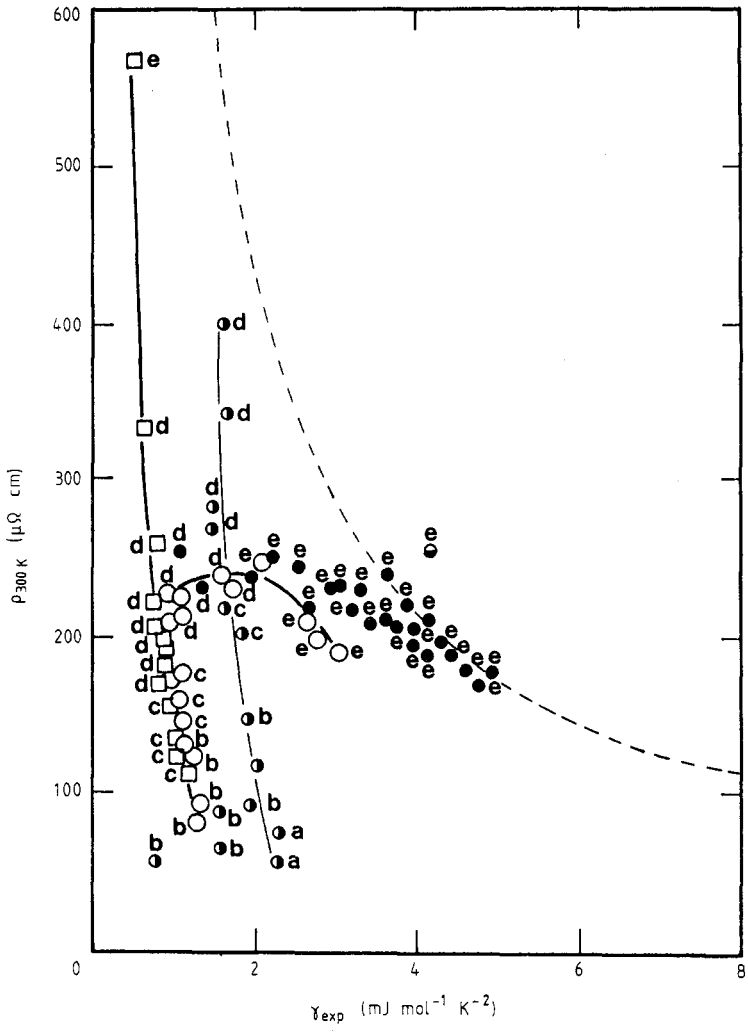

Figure 13. The resistivity at 300 K plotted against the electronic specific heat coefficient γ_{exp} for a number of non-magnetic amorphous alloys (the bold lower case letters **a–e** correspond to the curves A–E of figure 12): ○, $(Ni_{67}X_{33})_{1-x}Al_x$ (X ≡ Ti, Zr and La); □, Al–Ni–Si and Al–Ge–Ni; ◑, Ca–Mg–Al and Ca–Mg–Cu; ●, $(Ni_{33}Zr_{67})_{1-x}X_x$ (X ≡ B, Si, Al, Cu) and Cu–Zr–Al; ◒, Al–Y (see text); – – –, possible envelope, which represents the hyperbolic relation $\rho\gamma = 850$ where ρ is in microohms centimetres and γ is in millijoules per mole per kelvin squared. The value of 850 corresponds to the case $\Lambda_F = 4$ Å and $v_F = \frac{1}{5} \times 10^8$ cm s^{-1}.

path and $N(E_F)$ is the density of states at E_F. In the limiting case, where Λ_F reaches a possible minimum value limited by an average atomic distance of about 4–5 Å and v_F also approaches a possible minimum value, equation (1) leads to a unique situation such that the resistivity is solely determined by the magnitude of $N(E_F)$ or γ_{exp}; the higher $N(E_F)$, the lower is the resistivity.

Figure 13 shows the relationship between the measured values of ρ_{300K} and γ_{exp} for a large number of non-magnetic amorphous alloys so far studied, including the present Al-based alloys. (The bold lower case letters **a–e** correspond to curves A–E of figure 12.) It is apparent that an envelope (see broken curve in figure 13) exists across which

the data are scarcely found. The most important is the fact that the non-Boltzmann ρ–T curves of D and E appear only along the envelope and that the envelope is a good approximation to the inversely proportional relationship between ρ and $N(E_F)$. The latter indicates that the d electrons at the Fermi level predominantly participate in the electron conduction in such a high-resistivity regime. In other words, the Mott s–d scattering model, which predicts $\rho \propto N(E_F)$, does not hold. It may be also noted that the types A to C, which can be described in terms of the Boltzmann transport equation or the generalised Faber–Ziman theory, always appear well inside the envelope.

Let us now focus on the data for Al-based amorphous alloys in figure 13. The data for all Al–Si (or Ge)–Ni alloys, which are designated as the sp-electron system, fall on a steeply declining curve in the range of γ_{exp} below 1.5 mJ mol^{-1} K^{-2} and the ρ–T curve changes from curve B to curve E successively with increasing resistivity. This behaviour conforms well with the argument based on figure 12. The same feature has been observed in other sp-electron systems such as Ca–Mg–Al (Mizutani *et al* 1987a) and Ag–Cu–Ge (Mitzutani *et al* 1988). Type E occurs only when the resistivity reaches 500 $\mu\Omega$ cm in the sp-electron system. A sharp rise in the electrical resistivity far beyond the value expected from the Faber–Ziman theory in Al–Xi (or Ge)–Ni is naturally explained by the development of the covalent bonding between metalloid elements Si and Ge, which has already been discussed in connection with the soft-x-ray spectra shown in figure 5. The data for the metal–metal alloys $(Ni_{67}X_{33})_{1-x}Al_x$ with $x > 0.6$ also fall on the curve formed by Al–Si (or Ge)–Ni. This indicates that these Al-rich $(Ni_{67}X_{33})_{1-x}Al_x$ alloys can be treated as the sp-electron system from the viewpoint of electron transport as well.

As x is reduced below 0.6, however, the data points for $(Ni_{67}X_{33})_{1-x}Al_x$ alloys deviate from the above-mentioned curve and switch onto a different branch. These data on this branch are characterised by ρ–T curves D or E, which have been observed in common with all kinds of d-electron systems (Mizutani 1988a, b). In other words, the ρ–γ behaviour in figure 13 allows us to judge that the present $(Ni_{67}X_{33})_{1-x}Al_x$ amorphous alloys with $x < 0.6$ may well be designated to the d-electron system.

A brief comment may be made concerning other Al-based amorphous alloys. The resistivity for Ca–Mg is only around 50 $\mu\Omega$ cm but it increases rapidly on replacing Mg by Al (Mizutani *et al* 1987a). As a result, the ρ–γ data for the Al–Ca–Mg ternary alloys fall on a steeply declining curve almost parallel to that formed by the Al–Si (or Ge)–Ni and the ρ–T characteristics change successively from curve A to curve D with increasing resistivity. Only a single data point for the Al–Y amorphous alloy is also plotted in figure 13; the value of the resistivity is collected from the data reported by Trudeau and Cochrane (1989), whereas the value of γ from the data of Mizutani *et al* (1987b). The ρ–γ data point for the Al–Y alloy apparently falls slightly above the branch formed by many other d-electron alloys. Hence, further work is urgently needed to establish whether the critical boundary in the ρ–γ plot can be experimentally well defined. The electron transport in this limiting case is of great interest.

In summary, we should point out from the ρ–γ plot in figure 13 that there apparently exists a boundary beyond which data are no longer obtained. This means that a maximum resistivity is present for a given density of states at E_F; any resistivity at a given $N(E_F)$ cannot go beyond a value predicted from equation (1), provided that the shortest mean free path and a minimum average Fermi velocity exist. The minimum Fermi velocity of the d-electron system has been evaluated to be roughly one third to one fifth of the free-electron value of 10^8 cm s^{-1} and the minimum mean free path to be around 4 Å (Mizutani 1988a, b). The ordinary transport mechanism, described by the Boltzmann transport equation or the generalised Faber–Ziman theory, yields ρ–T curves A–C and the set of ρ- and γ-data fall well inside this critical envelope.

4.3. Hall coefficient

We now discuss the Hall coefficient data shown in figure 9. The broken curve represents the free-electron value calculated under the assumption that Ni, Al, Si and Ge donate 0, 3, 4 and 4 valence electrons/atom, respectively. The data for all Al-rich alloys are found to be close to the free-electron value, indicating the validity of the free-electron approach. However, a decrease in Al content in Al–Si(or Ge)–Ni leads to a deviation in the measured R_H towards a negative direction. This implies that the carrier density decreases rapidly with decreasing Al or increasing Si (or Ge) concentration. We can attribute this to the development of covalent bonding, the presence of which has already been discussed in connection with the Si Kβ soft-x-ray emission spectra (see figure 5). We consider that the interpretation in terms of the formation of covalent bonding is quite consistent with other experimental findings:

(i) a rapid fall of γ_{exp};
(ii) a sharp increase in ρ_{300K};
(iii) accompanying changes in ρ–T characteristics from curves A to E, as already discussed in § 4.2.

Bhatnagar *et al* (1989) recently carried out measurements of the electron transport properties including the Hall coefficient for the $(Ni_{36}Zr_{64})_{1-x}Al_x$ $(0 \leqslant x \leqslant 0.25)$ amorphous alloys and conjectured that the addition of Al to the Ni-rich alloys would lead to a large increase in the magnitude of R_H in the negative direction. As opposed to their conjecture, the Hall coefficient in $(Ni_{67}X_{33})_{1-x}Al_x$ (X ≡ Ti, Zr and La) reduces its magnitude and even becomes positive as x increases but resumes a negative value above $x = 0.7$. As a result, a sharp peak is formed at about $x = 0.6$, as shown in figure 9. A positive Hall coefficient has been observed in a number of d-electron systems (Gallagher *et al* 1983, Cochrane *et al* 1983, Schulte *et al* 1984, Mizutani *et al* 1987c, Yamada *et al* 1987a). Howson and Morgan (1985) have argued that a positive Hall coefficient arises from an anomalous dispersion of the free electrons, which is caused by the s–d hybridisation effect.

Nguyen Manh *et al* (1986) calculated the density of states for $Cu_{1-x}Zr_x$ amorphous alloys over the range $0.15 \leqslant x \leqslant 0.75$, using a standard tight-binding Hamiltonian including s–d hybridisation and tried to explain the sign reversal of the Hall coefficient by relating its sign to the energy derivative of the self-energy. They emphasised that the abrupt change in the electronic structure is responsible for the sign reversal, which occurs at about 15 at.% Zr in the Cu–Zr binary system. They revealed that, in this critical concentration range around 15 at.% Zr, the Fermi level located at the Zr 4d states moves to the very edge of the Zr 4d resonance states. This implies that the electronic structure at E_F changes from the d- to sp-electron-dominant states. Indeed, they noted that the density of states at E_F is decreased to 1.03 mJ mol^{-1} K^{-2} for 15 at.% Zr compared with 1.88 mJ mol^{-1} K^{-2} for 25 at.% Zr. As is clear from the preceding discussion, one immediately realises that such a change in the electronic structure has been proved to occur at $x = 0.6$ in the present $(Ni_{67}X_{33})_{1-x}Al_x$ (X ≡ Ti, Zr and La) amorphous alloy systems and that the sign reversal of the Hall coefficient apparently occurs in response to the change in the electronic structure from the sp- to d-electron system.

It may be of interest, at this stage, to plot available Hall coefficient data for the Zr-based binary and ternary amorphous alloys as a function of Zr concentration. The results are shown in figure 14, into which the present data are also incorporated. It can be seen that, regardless of an alloy system, a positive Hall coefficient appears as soon as Zr is added to about 5–15 at.%. At this critical concentration, the sp-electron-dominant

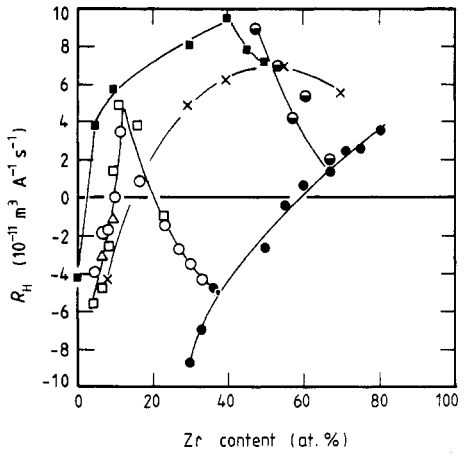

Figure 14. The Hall coefficient R_H as a function of Zr content for various Zr-based non-magnetic amorphous alloys: $(Ni_{67}X_{33})_{1-x}Al_x$ (X = Ti (□) and La (△)); ◑, $(Ni_{33}Zr_{67})_{1-x}Al_x$; ■, $Cu_{50}Zr_{50-x}Al_x$; ×, Cu–Zr; ●, Ni–Zr (see text).

electronic structure changes into that dominated by d electrons (Mizutani *et al* 1987c). With further increasing Zr concentration, the Hall coefficient in the ternary alloys eventually approaches the value for the corresponding TE-TL binary alloy and, hence, results in a sharp peak in the case of the $(Ni_{67}Zr_{33})_{1-x}Al_x$ ternary system, since $Ni_{67}Zr_{33}$ possesses a negative Hall coefficient. Within the context of the theory proposed by Nguyen Manh *et al*, the occurrence of such a sharp peak would be the direct consequence of a rapid change in the derivative of the density of states at E_F (Nguyen Manh *et al* 1987a, b).

4.4. Thermoelectric power

The sign of the Hall coefficient R_H has been discussed above in terms of the derivative of the density of states at E_F. According to the Mott s–d scattering model, the temperature coefficient of the thermoelectric power S also involves the derivative of the density of states at E_F as a major parameter. Hence, it is of interest to test whether there exists a correlation between these two physical quantities. The Al concentration dependence of R_H in figure 9 and S/T in figure 11 looks similar, suggesting the presence of some interrelation between them. However, we consider this similarity to be fortuitous. For instance, Bhatnager *et al* (1989) observed a decrease in S/T with increasing Al content in $(Ni_{36}Zr_{64})_{1-x}Al_x$ amorphous alloys, although a positive Hall coefficient in $Ni_{36}Zr_{64}$ (or $Ni_{33}Zr_{67}$) further increases in a positive direction upon adding Al (see figure 14). Hence, the Al concentration dependences of R_H and S/T in the Zr-rich alloys are entirely opposite to each other and offer a counter-example to the data for the Ni-rich alloys. Mizutani and Matsuda (1987) also pointed out the lack of correlation between S/T and the Hall coefficient by analysing the data for the simple metallic glasses such as Mg–Zn–Cu. Thus, we believe that there exists no universal correlation between the thermopower and the Hall coefficient in both d- and sp-electron systems. The interpretation of the thermopower (particularly, in the d-electron system) seems to be still elusive.

4.5. Crystallisation temperature

Matsuura and Mizutani (1986) discussed the crystallisation temperature of amorphous Ni–Zr alloys in terms of Lindemann's melting law

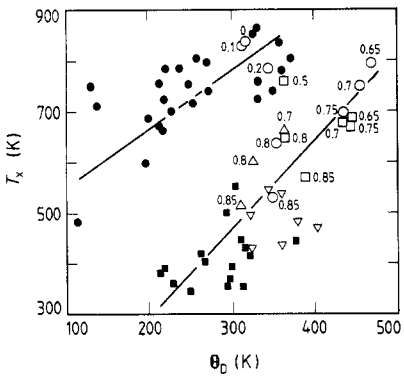

Figure 15. Crystallisation temperature T_x plotted against the Debye temperature for various non-magnetic amorphous alloys: □, $(Ni_{67}Ti_{33})_{1-x}Al_x$; ○, $(Ni_{67}Zr_{33})_{1-x}Al_x$; △, $(Ni_{67}La_{33})_{1-x}Al_x$; ▽, Al–Si(or Ge)–Ni. To avoid confusion, the remaining data are shown without explicitly mentioning individual alloy systems: ●, d-electron systems such as Ni–Zr, Ni–Ti and Cu–Zr; ■, sp-electron systems such as Ag–Cu–Mg, Ca–Mg–Al and Mg–Zn. The numbers in the figure indicate the Al concentrations x in $(Ni_{67}X_{33})_{1-x}Al_x$.

$$x_m = (3\hbar/\Theta_D)(T_m/Mk_B)^{1/2}(4\pi/3V)^{1/3} \tag{2}$$

where x_m is the ratio of the RMS displacement of atoms to the mean atomic radius, M is the atomic mass, V is the volume per atom and the other symbols carry their usual meanings. They noted that the value of x_m required for the initiation of the crystallisation always falls in the neighbourhood of 0.2, regardless of the alloy compositions. This suggests that the Debye temperature and the crystallisation temperature must be somehow interrelated. The values of T_x and Θ_D are plotted in figure 15 for various non-magnetic amorphous alloys, including both d-electron and sp-electron systems. The data for the Al-based amorphous alloys studied in these experiments are also incorporated. It can be seen that, in spite of rather large scatter of data points, d- and sp-electron systems separately constitute individual master lines having positive slopes. The crystallisation temperature for the d-electron system is universally higher than that for the sp-electron system, if a comparison is made at a given Debye temperature. Surprisingly, we find that this separation holds quite rigorously even in a given alloy system, i.e. in the present Al-based amorphous alloys. The separation of the present data into the two different master lines occurs precisely in accord with the change in the electronic structure. Hence, we consider this fact to be further evidence for the change in the electronic structure across $x = 0.6$: one region dominated by d electrons and the other dominated by sp electrons at the Fermi level.

5. Conclusion

We could determine from the low-temperature specific heat, XPS and soft-x-ray spectroscopy measurements the valence band structure near the Fermi level as a function of Al content for the $(Ni_{67}X_{33})_{1-x}Al_x$ (X ≡ Ti, Zr and La) and $Al_{100-x-y}Si_xNi_y$ ($10 \leqslant x \leqslant 35$, $10 \leqslant y \leqslant 20$) amorphous alloy systems. We revealed that the most striking feature is the fact that the electronic structure at the Fermi level changes from the d- to sp-electron-dominant states when the Al content exceeds $x = 0.6$ in metal–metal systems. The Al concentration dependence of the ρ–T characteristics in the range 2–300 K, the Hall coefficient and the crystallisation temperature is found to reflect directly the change in the electronic structure at the Fermi level.

It is also emphasised that the ρ–γ plot coupled with the ρ–T curves shown in figure 13 offers a very useful guide to the role of sp and d electrons as carriers, the regime where the ordinary Boltzmann-type scattering mechanism (figure 12, curves A–C) dominates and also the regime along the envelope, where the weak localisation effect becomes substantial (figure 12, curves D and E).

Acknowledgments

The authors are grateful to M Yamada, Nagoya Institute of Technology, for the XPS measurements and to N Kurachi, Aichi University of Education, for the thermoelectric power and the Hall coefficient measurements. Thanks are also given to H Komatsu, Tohoku University, for his assistance with the sample preparation by the sputtering technique.

References

Bhatnagar A K, Pan R and Naugle D G 1989 *Phys. Rev.* B **39** 12460
Cochrane R W, Destry J and Trudeau M 1983 *Phys. Rev.* B **27** 5955
Faber T E and Ziman J M 1965 *Phil. Mag.* **11** 153
Gallagher B L, Greig D, Howson M A and Croxon A A 1983 *J. Phys. F: Met. Phys.* **13** 119
Gasser J-G, Mayoufi M and Bellissent-Funel M-C 1989 *J. Phys.: Condens. Matter* **1** 2409
Howson M A and Morgan G J 1985 *Phil. Mag.* B **51** 439
Inoue A, Ohtera K, Tsai A P and Masumoto T 1988a *Japan. J. Appl. Phys.* **27** L280
—— 1988b *Japan. J. Appl. Phys.* **27** L479
Inoue A, Yamamoto M, Kimura H M and Masumoto T 1987 *J. Mater. Sci. Lett.* **6** 194
Matsuura M and Mizutani U 1986 *J. Phys. F: Met. Phys.* **16** L183
McMillan W L 1968 *Phys. Rev.* **167** 331
Mizutani U 1988a *Trans Japan. Inst. Met. Suppl.* **29** 275
—— 1988b *Mater. Sci. Eng.* **99** 165
Mizutani U and Matsuda T 1987 *J. Non-Cryst. Solids* **94** 345
Mizutani U, Sasaura M, Yamada Y and Matsuda T 1987a *J. Phys. F: Met. Phys.* **17** 667
Mizutani U, Sato K, Sakamoto I and Yonemitsu K 1988 *J. Phys. F: Met. Phys.* **18** 1995
Mizutani U, Tanaka M and Sato H 1987b *J. Phys. F: Met. Phys.* **17** 131
Mizutani U, Yamada Y, Mishima C and Matsuda T 1987c *Solid State Commun.* **62** 641
Nguyen Manh D, Mayou D, Cyrot-Lackmann F and Pasturel A 1987b *J. Phys. F: Met. Phys.* **17** 1309
Nguyen Manh D, Mayou D, Morgan G J and Pasturel A 1987a *J. Phys. F: Met. Phys.* **17** 999
Nguyen Manh D, Pavuna D, Cyrot-Lackmann F, Mayou D and Pasturel A 1986 *Phys. Rev.* B **33** 5920
Oelhafen P, Hauser E and Güntherodt H-J, 1980 *Solid State Commun.* **35** 1017
Sakamoto I, Yonemitsu K, Sato K and Mizutani U 1988 *J. Phys. F: Met. Phys.* **18** 2009
Schulte A, Eckert A, Fritsch G and Lüscher E 1984 *J. Phys. F: Met. Phys.* **14** 1877
Trudeau M L and Cochrane R W 1989 *Phys. Rev.* B **39** 13212
Tsai A P, Inoue A and Masumoto T 1988 *Metall. Trans.* A **19** 1369
Yamada Y, Itoh Y, Matsuda T and Mizutani U 1987b *J. Phys. F: Met. Phys.* **17** 2313
Yamada Y, Itoh Y, Mizutani U, Shibagaki N and Tanaka K 1987a *J. Phys. F: Met. Phys.* **17** 2303
Yamanaka E, Yamada Y, Ohara I, Matsuda T and Mizutani U 1988 *Trans. Japan. Inst. Met. Suppl.* **29** 329